International Journal of Earth, Energy and Environmental Sciences
ISSN: 2517-942X
Vol:9, No:5, 2015

Microstructural and Magnetic Properties of $Ni_{50}Mn_{39}Sn_{11}$ and $Ni_{50}Mn_{36}Sn_{14}$ Heusler Alloys

M. Nazmunnahar, J. J. Del Val, A. Vimmrova, J. González

***Abstract*—**We report the microstructural and magnetic properties of $Ni_{50}Mn_{39}Sn_{11}$ and $Ni_{50}Mn_{36}Sn_{14}$ ribbon Heusler alloys. Experimental results were obtained by differential scanning calorymetry, X-ray diffraction and vibrating sample magnetometry techniques. The Ni-Mn-Sn system undergoes a martensitic structural transformation in a wide temperature range. For example, for $Ni_{50}Mn_{39}Sn_{11}$ the start and finish temperatures of the martensitic and austenite phase transformation for ribbon alloy were M_s=336K, M_f=328K, A_s=335K and A_f=343K whereas no structural transformation is observed for $Ni_{50}Mn_{36}Sn_{14}$ alloys. Magnetic measurements show the typical ferromagnetic behavior with Curie temperature 207 K at low applied field of 50 Oe. The complex behavior exhibited by these Heusler alloys should be ascribed to the strong coupling between magnetism and structure, being their magnetic behavior determined by the distance between Mn atoms.

***Keywords*—**Structural transformation, as-cast ribbon, Heusler alloys, Magnetic properties.

I. Introduction

HUESLER alloys of Ni-Mn-Sn has attracted much attention for scientific research due to their magnetic field induced strain [1], [2] magnetic shape memory effect [3], [4] and potential application for magnetic refrigeration at room temperature [5]-[9]. These alloys have ability to undergo a reversible first-order martensitic transformation (MT) from a high-temperature cubic austenite phase to a structurally modulated martensite phase [10], [11]. By lowering the temperature a cubic high temperature parent austenite phase transforms into a tetragonal, orthorhombic, or monoclinic martensite ordered by domains (the martensite structure of which can be 10*M*, 14*M*, $L1_0$ or 4*O* depending on the alloy composition and manufacturing conditions). The complex behavior exhibited by this non-stoichiometric Ni-Mn-Sn Heusler alloy is due to the strong coupling between magnetism and structure, and also the magnetic ordering of these alloys strongly depends on the distance between Mn atoms [12]. By adding other elements such as Cu, Co, Al etc. [13]-[16] and changing fabrication conditions [17], [18] are common ways to understand the structural and magnetic properties of these alloys. The magnetic properties and magnetocaloric effects in Ni-Mn-Sn alloys were found to be very sensitive to their composition and fabrication conditions. Therefore systematic studies on these alloys are still needed. Recently, Maziarz et al. reported that by varying the Ni/Mn ratio of Ni-Mn-Sn alloy melt-spun ribbons show a heterogeneous microstructure [19]. However, in particular, the Ni-Mn-Sn alloy system is an interesting class of materials due to the reported large magnetocaloric effect [5]. A specific feature of these alloys is that the saturation magnetization is greatly reduced or becomes almost zero upon the structural transformation from austenite to martensite [20], [21].

In last years, rapid quenching is employed to produce a high quality Heusler alloys. As a rule, the high cooling rate during the solidification process promotes a more homogeneous distribution of elements in the alloys significantly reducing both the amount of minor secondary phases and the temperature and time of annealing needed to achieve a nearly single-phase material. Hernando et al. [17], [22] have reported the highly ordered columnar-like grains in melt spun Ni-Mn-Sn ribbons running through the ribbon thickness. N. H Dan et al. [23] reported that with appropriate compositions and annealing conditions, the Ni-Mn-Sn shows both the positive and negative entropy changes with quite large magnitude. Therefore, Ni-Mn-Sn system is of prospective importance as ferromagnetic shape memory alloy and promising magnetic refrigerant alloy. In this work, we have investigated microstructural and magnetic properties of $Ni_{50}Mn_{39}Sn_{11}$ and $Ni_{50}Mn_{36}Sn_{14}$ as-cast ribbons.

II. Experimental Details

As-cast ingots with a nominal composition of $Ni_{50}Mn_{50-x}Sn_x$ (x=11, and x=14) alloys (at %), were produced by arc melting, employing highly pure elements. The obtained ingots were annealed in evacuated quartz capsule for 24 h at 1173 K and subsequently cooled down at room temperature. Ribbon flakes 1.5-2.0 mm width, 70μm thickness and 4-5 mm length were produced by melt spinning in Ar atmosphere. The crystal structure was determined by X-ray diffraction (XRD) using CuKα radiation at room temperature, and the composition analysis was performed through Scanning Electron Microscopy (SEM, JEOL 6100) equipped with an Energy Dispersive X-ray microanalysis system (EDX, Inca Energy 200). Differential Scanning Calorimetry (DSC) measurements below room temperature was carried out in the DSC Q 2000 calorimeter with a liquid nitrogen cooling system in a heating and cooling rate of 5 K/min. Magnetic properties for ribbons were measured with PPMS system (QUANTUM DESIGN Inc.) by using the Vibrating Sample Magnetometer (VSM)

M. Nazmunnahar is with the Czech Technical University in Prague, Thakurova 7, 16629 Prague 6, Czech Republic (corresponding author to provide phone: +420-22435-712; fax: +420224355044; e-mail: nazu.nanoscience@gmail.com).

J. J. Del. Val and J. Gonzalezl are with the University of Basque Country, 1072, 20080 San Sebastian, Spain (e-mail: wapvaalj@sq.ehu.es, julianmaria.gonzalez@ehu.eus).

A. Vimmrova is with the Czech Technical University in Prague, Thakurova 7, 16629 Prague 6, Czech Republic (e-mail: vimmrova@fsv.cvut.cz).

technique between 5 K and 350 K with applied magnetic field ranging from 50 Oe up to 30 kOe. MT was characterized from thermomagnetic measurements, which means zero-field cooling (ZFC), field cooling (FC) and field heating (FH) routines that were performed using different applied magnetic fields.

III. Results and Discussion

A. Compositional Analysis

The ribbons of $Ni_{50}Mn_{50-x}Sn_x$ (x =11 and 14) alloys the chemical composition were determined by Scanning electron microscopy equipped with EDS method.

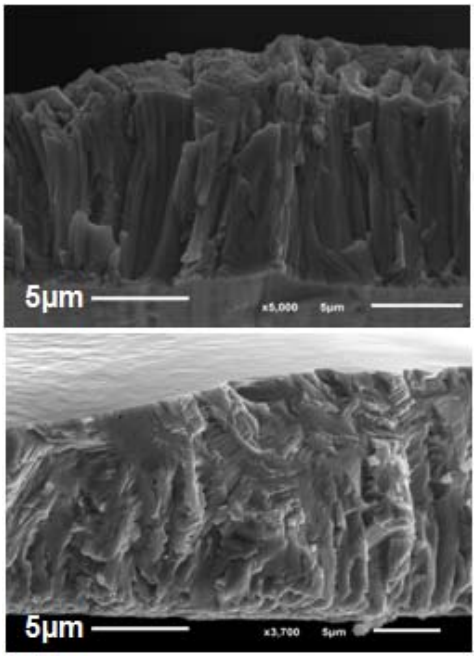

Fig. 1 SEM micrographs of as cast ribbons of $Ni_{50}Mn_{39}Sn_{11}$ (up) and $Ni_{50}Mn_{36}Sn_{14}$ (down)

Typical SEM images of fracture cross section and free surface of these as cast ribbons are presented in Fig. 1. Ordered columnar microstructure is observed in the cross section, indicating that the rapid solidification process induces theformation of textured polycrystalline ribbons [22], [24], [25]. Similar behavior has been reported in other Ni-Mn-Sn alloy [26].

An averaged composition of ribbon Ni51Mn36Sn13.1 (x=11) and Ni52.4Mn34.4Sn14.2 (x=14) has been found after a careful study carried out at different points of the sample. It is observed an appreciable shift of the nominal composition, which could cause changes in the magnetic properties with respect to this one. The estimated error in determining the concentration of each element is of ± 0.1%.

B. Calorimetric Studies

In order to characterize the martensitic transformation we have studied the thermal properties of $Ni_{50}Mn_{50-x}Sn_x$ (x=11 and 14) ribbon alloy series by DSC at a heating and cooling rate of 5 K/min in a liquid nitrogen cooling system.

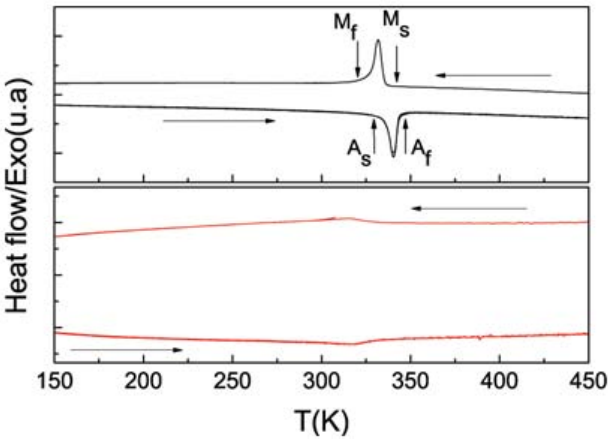

Fig. 2 DSC cycle scans for the alloy $Ni_{50}Mn_{39}Sn_{11}$(black) and $Ni_{50}Mn_{36}Sn_{14}$ (red) at heating and cooling rate of 5 K/min. Arrows indicate cooling (up: martensite to austenite) and heating (down: austenite to martensite)

Fig. 2 shows the DSC heating and cooling curves in $Ni_{50}Mn_{50-x}Sn_x$ (x=11and 14) for as ribbon alloys. The peaks of the as quenched ribbon (x=11) at % Sn content is clearly defined whereas the transformation peaks of the (x=14) at % Sn content tend to be diffused and extended on a wider temperature range. This is due to annealing and as quenching procedure. Similar behavior was found in as bulk Ni-Mn-Ga alloys [27]. The characteristic transition temperatures at which martensite start and finish for ribbons are (M_s, M_f), and austenite start and finish (A_s, A_f) and the width of the hysteresis ΔT determined as the difference between the temperatures corresponding to the peak positions of the forward and reverse temperatures are collected in Table I.

As can be seen from Fig. 2 for x=11, sharp exothermic and endothermic peaks which correspond to martensitic and reverse transformation, respectively, appear at around 220-350 K where the martensitic transformation starting (M_s) and finishing (A_f) temperatures are defined as the temperatures at which the extrapolation lines of those peaks and the base line cross. In addition, for $Ni_{50}Mn_{50-x}Sn_x$ (x=14) border peaks appear and it is difficult to observe the transformation temperatures for this alloys. The same effect has shown in NiMnX (x=In, Sn, Sb) ferromagnetic shape memory alloys [28]. The DSC signals obtained in the two thermal cycles are describing well the successive structural and magnetic transitions in these alloys. It is shown from the thermodynamics parameters given in Table I, the initial TM value has decreased from a value 340 K at x=11 at% Sn content. However, no TM value is seen at x=14 alloy.

As can be seen from DSC thermograms in Fig. 2 (up), the T_C and TM values have approached very close to each other so that only a single thermal signal arises out of a magnetostructural coupling. It is difficult to allocate TM values with such thermogram. These could be determined only

from thermomagnetic plots which will be discussed in the magnetic studies section. Obviously, the $Ni_{50}Mn_{50-x}Sn_x$ alloys, with x=11, show the martensite phase at room temperature, while the austenite phase appears at x=14, series alloys, the results obtained above from XRD analysis.

TABLE I
THE VALUES OF THE MARTENSITE AND AUSTENITE TRANSFORMATION TEMPERATURES AND WIDTH OF THE HYSTERESIS IN RIBBON $NI_{50}MN_{50-X}SN_X$ (X = 11 AND 14) ALLOYS DETERMINED FROM THE DSC THERMOGRAMS

Alloys	M_s /K	M_f /K	As /K	A_f /K	T_M /K	ΔT /K
$Ni_{50}Mn_{39}Sn_{11}$	336	328	335	343	340	7
$Ni_{50}Mn_{36}Sn_{14}$	.....	.....	.....	.....	.....	.....

C. Structural Analysis

Fig. 3 shows the x-ray diffraction patterns of $Ni_{50}Mn_{50-x}Sn_x$ (x=11 and 14) ribbon alloys at room temperature (RT).

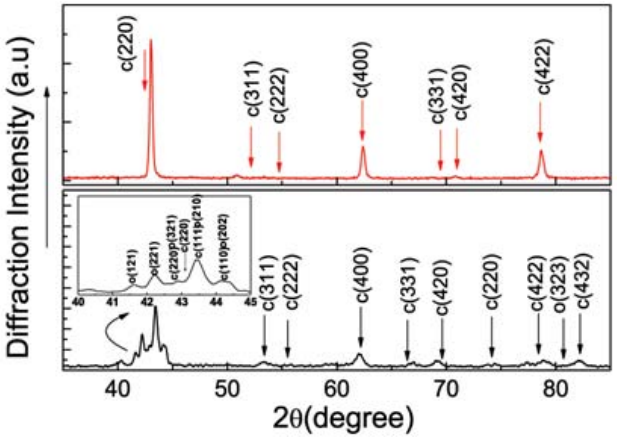

Fig. 3 X-ray diffraction patterns from martensite to austenite of $Ni_{50}Mn_{39}Sn_{11}$ (down) and $Ni_{50}Mn_{36}Sn_{14}$ (up)

It can be noted that the first alloy (x=11), display one kind of pattern while the other alloy (x=14) show another kind of pattern. As seen in Fig. 3 the alloys with x=11 shows the presence of mixed martensite and austenite phases at RT, while the other alloy (x=14) present an austenite phase. The inset shows the details in the range $400 \leq 2\theta \leq 460$.The martensite phase is indexed as an orthombic structure while the austenite phase is indexed as a cubic $L2_1$ structure. In Fig. 3 the miller indices (hkl) c and (hkl) o denotes the peaks in the $L2_1$ cubic and (Pmma) orthombic structure of the alloys respectively. The lattice parameter ac is calculated to be 0.598 nm for $Ni_{50}Mn_{39}Sn_{11}$ alloy and 0.0659 nm for $Ni_{50}Mn_{36}Sn_{14}$ alloy in the austenite phase. The presence of super lattice reflections (111) and (311) suggests that the alloys are crystallized in the highly ordered cubic $L2_1$ Heusler structure. The same results have been found for $Ni_{50-x}Mn_{37+x}Sn_{13}$ alloys [29].

It can be seen that decreasing Mn content or increasing Sn content for $Ni_{50}Mn_{50-x}Sn_x$ (x=11 and 14) alloy stabilizes the austenite phase at RT or in other words, an increase in Ni/Mn and Mn/Sn ratio suppresses the martensite phase and favors the formation of the austenite phase at RT. Moreover the intensity of (220) c peak is increasing by varing the x content from 11 to 14 in the $Ni_{50}Mn_{50-x}Sn_x$ alloys. As can be seen the poor intensity in this (220) c peak in the alloy consisting of x=11 is increasing regularly upon increasing the x-content to as large as 14. The specific peak becomes the most intense reflection in the XRD patterns in Fig. 3 upon martensite → austenite phase transformation in the $Ni_{50}Mn_{50-x}Sn_x$ (x=11 and 14) at% Sn content.

D. Magnetization Studies

M (T) for $Ni_{50}Mn_{50-x}Sn_x$ (x=11, and 14) ribbon samples is presented in Figs. 4 and 5. For M (T) the data have been recorded for zero field cooled (ZFC), field cooling (FC), and field heating (FH) protocols in presence of different applied magnetic fields from 50 Oe to 30 kOe up to maximum temperature of 350 K. Fig. 4 shows M (T) for the sample with x=11, and 14 for applied magnetic field of 50 Oe. At 50 Oe the sample with x=11 no structural transformation has been observed. In addition M (T) for the applied field of 1 kOe to 30 kOe is shown in Fig. 5.

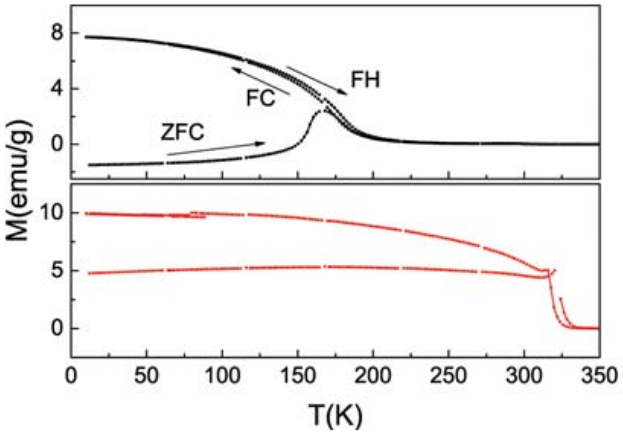

Fig. 4 ZFC, FC and FH thermo-magnetic curves of $Ni_{50}Mn_{39}Sn_{11}$ (up) and $Ni_{50}Mn_{36}Sn_{14}$ (down) at H=50Oe. Arrows indicate cooling and heating regimes

The behavior of the M (T) for the both samples is that of a typical ferromagnetic with a curie temperature T_c=207 K. Since M (T) measurements are restricted to the maximum temperature of 350 K, the full hysteresis due to M (T) is only visible above this temperature range. A partial (minor) loop is seen for the x=11 sample, at 10 kOe and 30 kOe magnetic field. While no loop is present for the x=14 as the MT for these samples are well above 350 K. This is supported by the observation of pure martensite Orthombic phase in the x-ray diffraction at room temperature for that x=11 of the Ni_{50} series samples. If we look carefully on the M (T) behavior of x=11 sample, a dip is observed within the region of MT. similar dip has been observed in some other FSMAs within the region of MT [6], [30]. It has been interpreted due to the existence of two critical temperatures corresponding to the FM phases of martensite and austenite. In certain situations, it might happen, particularly when TM is close to the T_c of the austenite phase, the martensite T_C may separate out from. As Mn is substituted

for Sn, excess Mn atoms occupy Sn sites. In such spatial configurations, Mn atoms can have Mn atoms as nearest neighbors along the (110) directions. The Mn-Mn spacing, in this case, is similar than that in the stoichiometric compound and is, therefore, expected to in traduce AF exchange leading to local nonlinear spin structures which can pin the FM domains in different configurations depending on whether the sample is cooled through T_c in an external field or not.

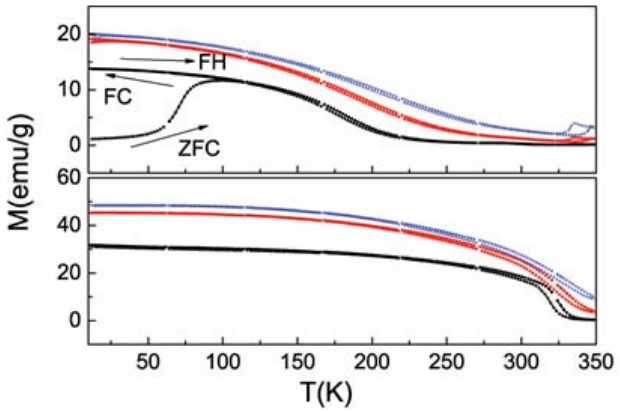

Fig. 5 ZFC, FC and FH thermo-magnetic curves of $Ni_{50}Mn_{39}Sn_{11}$ (up) and $Ni_{50}Mn_{36}Sn_{14}$ (down) at H=1 kOe(black), 10 kOe(red) and 30 kOe (blue). Arrows indicate cooling and heating regimes.

It has been shown that a partial substition of Sn for Mn in $Ni_{50}Mn_{50-x}Sn_x$ alloys by x=11 and 14 leads to shift the value in the high temperature austenite phase to 207 K and 320 K, respectively. As can be seen that for $Ni_{50}Mn_{50-x}Sn_x$ (x=11 and 14) the T_c value is increase with increase the Sn content as well as decrease the valance electron concentration. Similar results have been reported in other Ni-Mn-X (x=In, Sn, Sb) Heusler alloys [20], [31].

E. Hysteresis Behavior

The ferromagnetic nature of the as cast ribbons is evidences from the magnetization (M) versus (H) curves taken at different temperatures, as shown in Figs. 6 (a), (b) for $Ni_{50}Mn_{50-x}Sn_x$ (x=11 and 14). The measurements were carried out by cooling the sample from 375 K down to the required temperature of interest zero fields and then varying the field from 0 to 5 *T*.

Inset of Figs. 6 (a), (b) shows the low field region of the M-H loops, showing coercivity (H_c) of about 51 Oe, 22 Oe, and remanent magnetization (M_r) of about 2.359 emu/g, and 2.589 emu/g at 150 K for x=11, and 14 respectively. In addition the coercivity (H_c) of about 13 Oe and remanent magnetization of about 1.265 emu/g at 220 K for x=14 respectively. The values of H_c and M_r of the martensite phase at low temperature (150 K) are found to be higher than that of austenite phase at high temperature (220 K). The higher values H_c and M_r at low temperatures is attributed to the fact that low temperature twinned martensite phase is more disordered phase compared to the ordered austenite phase, which occurs at high temperature. Similar behavior has been reported for Ni-Mn-Sn alloys [32]. Since martensite phase is a disordered and low temperature phase, it possesses lesser energy than that of austenite phase. Therefore, the value of H_c, required for complete reversal of magnetization and M_r is higher at low temperatures [33]. As can be seen, as temperature increases, the twin variants gets sufficient energy and less driving force is required for transformation from martensite to austenite phase due to which the value of H_c and M_r decreases at high temperature, i.e., in austenite phase.

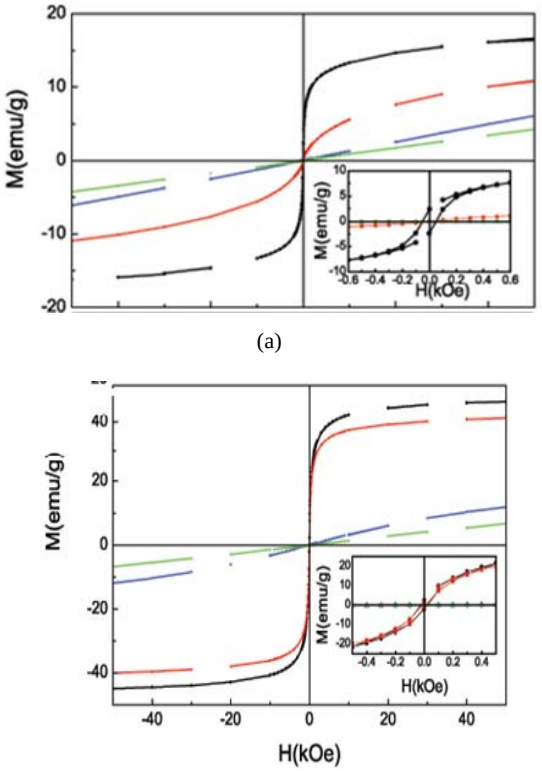

Fig. 6 (a), (b) *M vs H* plot for $Ni_{50}Mn_{39}Sn_{11}$ (up) and $Ni_{50}Mn_{36}Sn_{14}$ (down) at 150 K (black), 220 K (red) 350 K (blue) and 375 K (green) at applied field of 5*T*

At 150 K temperature the magnetization saturates at low temperature, and at 220K the saturation weakens leading to finite high field susceptibility. The *M (H)* data at 350 K and 370K, which corresponds to the paramagnetic state, shows a linear behavior whereas below this temperature, the curve is nonlinear and exhibits a small coercivity in the hysteresis. The Magnetization loops show small hysteresis at all the measured temperatures. This reflects that the sample is a soft ferromagnetic both in the austenite and martensite phase.

At higher temperatures 350 K and 375 K, in the austenite state, the sample is paramagnetic and orders ferromagnetically below T_C^A=305 K. As Mn is substituted for Sn, excess Mn atoms occupy Sn sites. As a results Mn-Mn spacing decreases which in turn introduce antiferromagnetic exchange. The *M-H* curve do not saturate even at low temperature 150 K, owing to the presents of antiferromagnetic exchange. The lack of

saturation in magnetization can be seen more pronounced in samples x=11 at% of Sn contents with higher Mn concentration. The coexistence of antiferromagnetic exchange within the ferromagnetic matrix due to excess Mn in the crystal structure is an essential source of nonsaturation. At higher Mn concentrations, long range ferromagnetic ordering weakens appreciably. This can be seen in the *M-H* curves of $Ni_{50}Mn_{39}Sn_{11}$ and in Figs. 6 (a), (b). The magnetizations of these samples are observed to be smaller in magnitude than that of $Ni_{50}Mn_{36}Sn_{14}$ (x=14) samples which have well defined ferromagnetic ground state (Figs. 6 (a), (b)). At 350 K and 375 K (above the T_C^M), M-H curve is linear, the data deviates from linearity due to the presence of short range ferromagnetic correlations. The *M-H* curves were observed to be linear at high temperature 350 K and 375 K for all the samples whereas below this temperature 150 K and 220 K, the curve is nonlinear and exhibits a small coercivity in the hysteresis. This nonlinear behavior at 150 K and 220 K is attributed to the short range ferromagnetic correlations in the alloys.

IV. Conclusion

Structural and magnetic transitions in Ni-Mn-Sn ribbon alloys have been studied. The effect of varying either Ni/Mn or Mn/Sn on the structural transition temperature was found to be the same. The increment in magnetization around structural transition points to the fact that the Heusler alloy here studied could be of potential interest in multifunctional applications such as actuator and or magnetocaloric material if proper composition is chosen. For wider utilization it would be necessary to improve namely the structural and magnetic properties, e.g. by adding the composition such as Cu, Co, Al etc. More works in this regard are now in progress.

Acknowledgment

Authors are thankful to Spanish MINECO for financial support under projects MAT2013-48054-C2-2-R, MAT2013-4731-C2-1, 2-P and Basque Government for a grant of ETORTEK programme (Strategic project inanoGune ii).

This publication was supported by the European social fund within the framework of realizing the project “Support of inter-sectoral mobility and quality enhancement of research teamsatCzechTechnicalUniversityinPrague,CZ.1.07/2.3.00/30.0034.

References

[1] R. Kainuma, Y. Imano, W. Ito, Y. Sutou, H. Morito, S. Okamoto, O. Kitakami, K. Oikawa, A. Fujita, T. Kanomata, K. Ishida, Nature 439(2006) 957-960.
[2] H. E. Karaca, I. Karaman, B. Basaran, Y. I. Chumlyakov, H. J. Maier, Acta materialia 54(2006) 233-245.
[3] R. Kainuma, Y. Imano, W. Ilto, H. Morito, Y. Sutou, K. Oikawa, A. Fujita, K. Ishida, S. Okamoto, K. Oikawa, T. Kanomata, Appl. Phys. Lett. 88 (2006)192513.
[4] Wu. Wang, Jinke Yu, Qijie Zhai, Zhiping Luo, Hongxing Zheng; J. Magne. and Magne. Materials 346(2013) 103-106.
[5] T. Krenke, E. Duman, M. Acet, E. F. Waserman, X. Moya, L. Manosa, A, Planes, Nat. Mater.4(2005)450
[6] T. Krenke, M. Acet, E. F. Wassermann, X. Moya, L. Mañosa, A. Planes, Phys. Rev. B 72(2005) 014412.
[7] Y. B. Yang, X. B. Ma, X. G. Chen, J. Z. Wei, R. Wu, J. Z. Han, H. L. Du, C. S. Wang, S. Q. Liu, Y. C. Yang, Y. Zhang, J. B. Yang, J. Appl. Phys. 111(2012) 07A916.
[8] E. C. Passamani, V. P. Nascimento, C. Larica, A. Y. Takeuchi, A. L. Alves, J. R. Provetib, M. C. Pereirac, J. D. Fabrisd, J. Alloys Compd. 509(2011) 7826.
[9] T. L. Phan, N. H. Duc, N. H. Yen, P. T. Thanh, N. H. Dan, P. Zhang, S. C. Yu, IEEE Trans. Magn. 48(2012) 1381.
[10] A. Planes, L. Mañosa, M. Acet. J. Phys.: Condens. Matter. 21, (2009) 233201.
[11] D. Y. Cong, S. Roth, M. Pötschke, C. Hürrich, L. Schultz, Appl. Phys. Lett. 97, (2010) 021908.
[12] A. Planes, Physics 3, (2010)36.
[13] T. Krenke, E. Duman, M. Acet, X. Moya, L. Mañosa, A. Planes, J. Appl. Phys. 102 (2007) 033903.
[14] R. Y. Umetsu, A. Fujita, W. Ito, T. Kanomata, R. Kainuma, J. Phys. Conden. Matter 23 (2011) 326001.
[15] Z. Zhong, S. Ma, D. Wang, Y. Du, J. Mater. Sci. Technol 28 (2012) 193
[16] V. Basso, C. P. Sasso, K. P. Skokov, O. Gutfleisch, V. V. Khovaylo, Phys. Rev. B85 (2012) 014430.
[17] B. Hernando, J. L. Sánchez Llamazares, J. D. Santos, V. M. Prida, D. Baldomir, D. Serantes, R. Varga, J. González, Appl. Phys. Lett. 92(2008) 13250.
[18] S. E. Muthu, N. V. R. Rao, M. M. Raja, S. Arumugam, K. Matsubayasi, Y. Uwatoko, J. Appl. Phys. 110 (2011) 083902.
[19] W. Maziarz, P. Czaja, M. J. Szczerba, L. Litynska-Dobrzynska, T. Czeppe, J. Dutkiewicz, J. Alloys Comp. 615, (2014) S173.
[20] T. Krenke, M. Acet, E. F. Wassermann, X. Moya, L. Mañosa, A. Planes, Phys. Rev. B 73, (2006) 174413.
[21] V. V. Khovaylo, K. P. Skokov, O. Gutfleisch, H. Miki, T. Takagi, T. Kanomata, V. V. Koledov, V. V. Shavrov, G. Wang, E. Palacios, J. Bartolomé, R. Burriel, Phys. Rev. B 81, (2010) 214406.
[22] B. Hernando, J. L. Sanchez Llamazares, J. D. Santos, L I Escoda, J. J. Suñol, R. Varga, D. Baldomir, D. Serantes, Appl. Phy. Lett. 92, (2008) 042504.
[23] N. H. Dan, N. H. Duc, N. H. Yen, P. T. Thanh, L. V. Bau N. M. An, D. T. K. Anh, N. A. Bang, N. T. Mai, P. K. Anh, T. D. Thanh, T. L. Phan, S. C. Yu, J. Magn. Mag Mate. 374, (2015) 372.
[24] J. L. Sánchez Llamazares, T. Sanchez .T, J. D. Santos, M. J. Pérez, M. L. Sanchez, B. Hernando, LI. Escoda, J. J. Suñol, and R. Varga, Appl. Phys. Lett. 92 (2008) 012513.
[25] J. D. Santos, T. Sanchez, P. Alvarez, M.L. Sanchez, J. L. Sánchez Llamazares, B. Hernando, LI. Escoda. LI, J. J. Suñol, and R. Varga, J. Appl. Phys. 103 (2008) 07B326.
[26] H. C. Xuan, K. X. Xie, D. H. Wang, Z. D. Han, C. L. Zhang, B. X. Gu, and Y. W. Du; Appl Phys Lett 92 (2008) 242506.
[27] K. Pushpanathan, R. Chokkalingam, R. Senthurpandi, R. Mahendran, Mater. Manufact. Proc.26 (2011)223.
[28] Y. Sutou, Y. Imano, N. Koeda, T. Omori, R. Kainuma, K. Ishida, K. Oikawa, Appl. Phys. Lett. 85 (2004)4358.
[29] S. Esakki Muthu, N. V. Rama Rao, M. Manivel Raja, D. M. Raj Kumar, D. Mohan Radheep, and S. Arumugam, Appl. Phys. Lett. 43 (2010) 425002.
[30] V. D. Buchelnikov, P. Entel, S. V. Taskaev, V. V. Sokolovskiy, A. Hucht, M. Ogura, H. Akai, M. E. Gruner and S. K. Nayak, Phys. Rev. B 72 (2008) 184427.
[31] B. Ingale, R. Gopalan, M. Manivel Raja, V. Chandrasekaran. and S. Ram, J. Appl. Phys., 102 (2007) 013906.
[32] X. Moya, L. Ma˜nosa, A. Planes, S. Aksoy, M. Acet, E. Wassermann, T. Krenke, Adv. Mate. Res., 52 (2008)189.
[33] R. Vishnoi and D. Kaur, J. Appl. Phys. 107 (2010)103907.